Improving Compositional Accuracy in APT Analysis of Carbides Using a Decreased Detection Efficiency

Downloaded from: https://research.chalmers.se, 2024-04-17 15:59 UTC

Citation for the original published paper (version of record):
Shinde, D., Thuvander, M., Rehan, A. et al (2019). Improving Compositional Accuracy in APT Analysis of Carbides Using a Decreased Detection Efficiency. Microscopy and Microanalysis, 25(2): 454-461.
http://dx.doi.org/10.1017/S1431927619000424

N.B. When citing this work, cite the original published paper.

research.chalmers.se offers the possibility of retrieving research publications produced at Chalmers University of Technology. It covers all kind of research output: articles, dissertations, conference papers, reports etc. since 2004. research.chalmers.se is administrated and maintained by Chalmers Library

(article starts on next page)

Microscopy and Microanalysis (2019), **25**, 454–461
doi:10.1017/S1431927619000424

Microscopy AND Microanalysis

Original Article

Improving Compositional Accuracy in APT Analysis of Carbides Using a Decreased Detection Efficiency

Mattias Thuvander[1]*, Deodatta Shinde[1], Arbab Rehan[2], Sebastian Ejnermark[2] and Krystyna Stiller[1]
[1]Chalmers University of Technology, SE-41296 Göteborg, Sweden and [2]Uddeholms AB, SE-68333 Hagfors, Sweden

Abstract

The composition of carbides in steel, measured by atom probe tomography, can be influenced by limitations in the ion detector system. When carbides are analyzed, many ions tend to field evaporate from the same region of the specimen during the same laser or voltage pulse. This results in a so-called multiple event, meaning that several ions impact the detector in close proximity both in time and space. Due to a finite detector dead-time not all ions can be detected, a phenomenon known as detector pile-up. The evaporation behavior of carbon is often different than the evaporation behavior of metals when analyzing alloy carbides, leading to preferential loss of carbon ions, and a measured carbon concentration below the expected value. This effect becomes stronger as the overall detection efficiency gets higher. Here, the detection efficiency was deliberately reduced by inserting a grid into the flight-path, which resulted in a higher and more correct carbon concentration, accompanied by an increase in the statistical uncertainty.

Key words: atom probe tomography, carbides, detection efficiency, multiple hits, quantification

(Received 10 September 2018; revised 25 February 2019; accepted 14 March 2019)

Introduction

Atom probe tomography (APT) is a useful technique for measuring local composition on a nanometer scale. The method relies on identifying, by time-of-flight mass spectroscopy, and positioning individual atoms that have been ionized by field evaporation from the tip of a needle-shaped specimen (Miller & Forbes, 2014). The specimen is held at a high DC potential and field evaporation is initiated by either a voltage pulse or a laser pulse that also serves as the start signal for the time-of-flight measurement. The detector consists of a channel plate, which turns the incoming ion to an electron burst, and a delay-line for positioning the electron burst. The *x*- and *y*-coordinates are obtained from timing signals from two crossed delay-lines, and commonly a third delay-line (at 45°) is used for redundancy (Jagutzki et al., 2002). The position of the atom in the specimen is calculated from the impact position on the detector using a reconstruction algorithm, basically assuming a point-projection, with some further modifications (Gault et al., 2012). The detection efficiency is mainly governed by the open area ratio of the channel plate, but the pulse handling electronics and algorithms also have an influence, which varies, depending on the design of the instrument, and today it ranges from ∼37 to ∼80% for the commercially available ones (Prosa et al., 2014; Martin et al., 2017). The most common type of channel plate has an open area ratio of about 60%, but channel plates with 90% have become available in recent years (Matoba et al., 2012). Many instruments are equipped with a so-called reflectron for improved mass resolution when using voltage pulsing, which typically decreases the detection efficiency further, as it consists of a wire mesh, with a transmission below unity, that the ions pass twice.

Obviously, it is desirable to have as high a detection efficiency as practical, to obtain a reconstruction that resembles the real material as closely as possible. The uncertainty in composition originating from counting statistics becomes smaller as the detection efficiency is increased, and thereby it becomes possible to determine the composition of very small features in the microstructure. In some cases, though, the accuracy of concentration measurements is significantly reduced, for example when analyzing carbides (Thuvander et al., 2011), nitrides (Tang et al., 2010), silicides (Kinno et al., 2012), or semiconductors (Müller et al., 2011). In the case of carbides, the main reason why the measured carbon concentration is usually too low is the limited capability of the detector system to register all ions from the same pulse, resulting in losses due to detector pile-up. The ions have a strong tendency of being field evaporated in groups, which results in several ions hitting the detector in close proximity to each other and within a very short time span. The fraction of carbon ions in these multiple hit events is higher than expected from the concentration, leading to a preferential loss of C in the analysis. In the case of cementite (Fe_3C), however, the measured C concentration is often too high, but in this case the deviation has also been attributed to preferential loss of Fe ions (Marceau et al., 2013).

*Author for correspondence: Mattias Thuvander,
E-mail: mattias.thuvander@chalmers.se

Cite this article: Thuvander M, Shinde D, Rehan A, Ejnermark S, Stiller K (2019) Improving Compositional Accuracy in APT Analysis of Carbides Using a Decreased Detection Efficiency. *Microsc Microanal* **25**, 454–461. doi:10.1017/S1431927619000424

Copyright © Microscopy Society of America 2019. This is an Open Access article, distributed under the terms of the Creative Commons Attribution licence (http://creativecommons.org/licenses/by/4.0/), which permits unrestricted re-use, distribution, and reproduction in any medium, provided the original work is properly cited.

Downloaded from https://www.cambridge.org/core. Chalmers Tekniska Högskola, on 02 Mar 2022 at 11:31:00, subject to the Cambridge Core terms of use, available at https://www.cambridge.org/core/terms. https://doi.org/10.1017/S1431927619000424

Another element that is strongly affected by multiple events is boron (Da Costa et al., 2012; Meisenkothen et al., 2015). The dead-time of the detector, together with the efficiency of the process to resolve multiple hits, are the factors governing the severity of the effect.

In some cases, it is possible to use only isotopes of low, and known, abundance for quantification, as the probability is low that more than one such ion from a single pulse hits the detector. This has been demonstrated for the analysis of carbides, using the ^{13}C isotope (Thuvander et al., 2011). An elegant statistical correction method for determining isotope abundance ratios, even in the presence of detector pile-up effects, was developed by Stephan et al. (2015), but it is not straightforward to implement this method for analyses containing multiple phases and elements. For the older 1D atom probe technique, a correction method based on measurement of the time difference of detected pairs was presented by Rolander & Andrén (1989), but this method cannot easily be applied to 3D APT. To some extent it is possible to decrease the fraction of multiple events by changing the analysis conditions. When using laser pulsing, the fraction decreases slightly if the laser pulse energy is increased, as shown for Ti(C, N) (Angseryd et al., 2011) and Ti–Si–N (Tang et al., 2010).

Yao et al. (2012) have investigated the nature of the detected multiple events. It was shown that the C ions comprising a multiple hit were typically separated by <5 nm, when analyzing a low-alloyed steel, and similar results have also been observed for WC (Thuvander et al., 2013). Yao et al. also observed a strong crystallographic dependence on the positions of C ions from multiple events. The influence of crystallography on the field evaporation behavior of an Al-alloy was also studied by De Geuser and co-workers. They concluded that the multiple events were caused by correlated evaporation, particularly at low-indexed poles (De Geuser et al., 2007). The possibility of extracting information from the multiple hit events has been investigated in detail by Saxey, who also observed molecular dissociation among the multiple hit events in GaN (Saxey, 2011).

The number of multiple hits and the number of ions detected in multiple hit events increase as the detection efficiency increases (Thuvander et al., 2013; Peng et al., 2018). Therefore, the negative effects of multiple events can be mitigated by decreasing the detection efficiency. This was demonstrated by Thuvander et al. when they inserted a fine-meshed grid in the flight path of the instrument, giving a detection efficiency of only 5%, and thereby the measured concentration of C in WC increased from 48.2 to 49.8 at.%, while the fraction of multiple events decreased from 47 to 9% (Thuvander et al., 2013). In that case, a large grain of WC was analyzed, so the decrease in the number of detected atoms had a negligible influence on the precision of the measured C concentration. In the current paper, the possibility of using the same approach for increasing the measured C concentration in APT analysis of small secondary MC carbides is explored. An increased C concentration, from 26 to 35%, was also observed when comparing two types of instruments with a detection efficiency of 52 and 37%, respectively (Martin et al., 2017). In their study, small precipitates of M_2C were analyzed. The motivation for improving the quantitative measurement of C in steel carbides is to both be able to determine the type of carbide, and measure any sub-stoichiometry, which is very challenging. Another area where minimizing the effect of detector pile-up is important, is for determining the isotopic ratio in meteoritic nanodiamonds (Heck et al., 2014; Lewis et al., 2015).

Materials and Methods

Two tool steels, A and B, were analyzed in this study. Steel A had the composition 0.3Si–1.7Cr–1.1Mn–2.7Mo–1.1V–0.4C and steel B 0.3Si–2.6Cr–0.8Mn–2.2Mo–0.9V–0.4C (wt%). After austenization, the steels were tempered to form secondary carbides. Steel A was tempered according to the scheme 2×2 h at 630°C plus 30 h at 650°C, in order to form relatively large secondary carbides. Steel B was tempered 2×2 h at 625°C to form small secondary carbides. The secondary carbides can principally be MC (based on VC) and M_2C (based on Mo_2C), but no separation into two populations was observed in the APT analyses, and it is assumed that all analyzed secondary carbides are MC, containing roughly the same amount of V and Mo, with a small addition of Cr. In this type of steel, M_2C typically has a much higher Mo/V ratio than was observed for the carbides in this study (Andersson, 2011), and also the measured C concentration should be lower, below 33 at.% due to detector pile-up. The C concentration of binary VC at 600–700°C can be in the range of about 45–47 at.%, from the binary phase diagram (Toth, 1971).

A standard Si(Sb) sample [a so-called pre-sharpened microtip (PSM) array] from CAMECA was used for checking the influence of using a grid-local electrode (GLE) on the detector hit map (also called desorption or evaporation maps), and also for demonstrating the effect of detection rate on the evaporation field.

The steels were ground to a thickness of 0.3 mm, and blanks with dimensions of $0.3 \times 0.3 \times 15$ mm^3 were cut using a low-speed saw. Needle-shaped specimens for APT were prepared using the standard two-step electropolishing method (Miller & Forbes, 2014). In the first step a neck was formed using a floating layer electrolyte consisting of 10% perchloric acid in 20% glycerol and 70% methanol on top of Galden®. In the second step, the whole blank was electropolished in 2% perchloric acid in 2-butoxyethanol until the blank parted at the position of the neck, resulting in an automatic turn-off of the current, giving two needle-shaped specimens. Finally, the specimens were electropolished using short pulses (2 ms) in the second electrolyte, in order to remove any residue at the surface. In all electropolishing steps the voltage was 18–20 V.

The instrument used was a LEAP 3000X HR (Imago Scientific Instruments, Madison, WI, USA). As the specimens are prone to fracturing during voltage pulsing, presumably because of the presence of carbides, the analyses were performed in laser pulsing mode with a laser pulse energy of 0.30 nJ, with the temperature

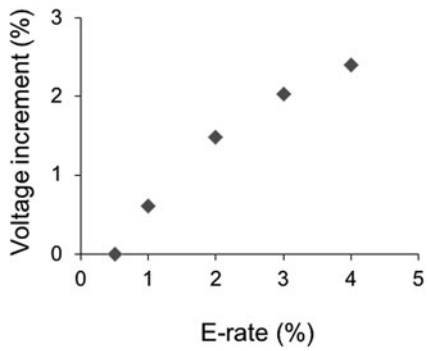

Fig. 1. Effect of evaporation rate on the voltage (evaporation field), from analyses of Si(Sb) standard PSM sample.

Downloaded from https://www.cambridge.org/core. Chalmers Tekniska Högskola, on 02 Mar 2022 at 11:31:00, subject to the Cambridge Core terms of use, available at https://www.cambridge.org/core/terms. https://doi.org/10.1017/S1431927619000424

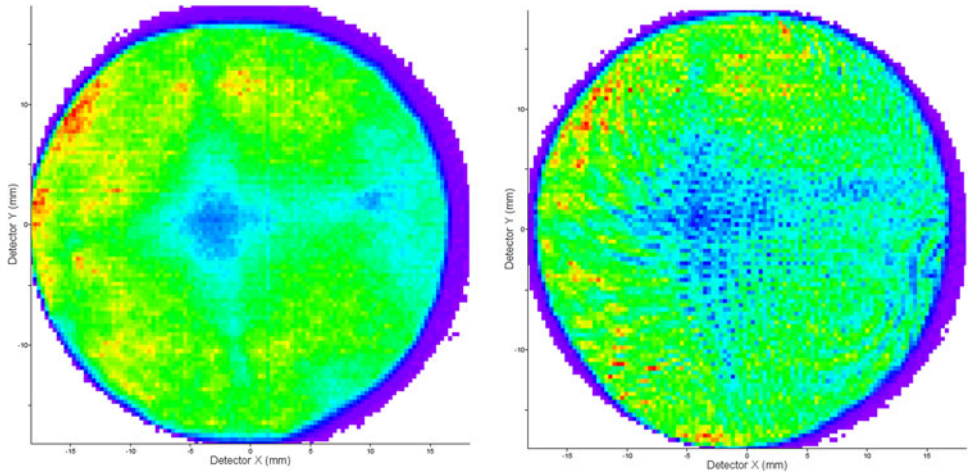

Fig. 2. Detector hit maps from two analyses of Si(Sb) using an NLE assembly (left) and the GLE40 assembly (right).

set at 50 K. The pulse frequency was 200 kHz. The influence of using laser mode instead of voltage mode is usually to decrease the fraction of multiple events (Thuvander et al., 2011, 2013), although the fraction of multiples can be high also for laser mode (Tang et al., 2010; Angseryd et al., 2011; Peng et al., 2017).

In order to vary the detection efficiency, two different types of local electrode assemblies were used. First, a normal local electrode (NLE) was used, giving the normal detection efficiency of 37%, specified by the supplier. Second, a GLE assembly was used, where a fine grid (mesh) was mounted at the exit side of the assembly (the so-called *puck*). The mesh has an open area of 14%, giving a detection efficiency of only 5%. The GLE used to analyze steel A is identical to the one used in a previous study (Thuvander et al., 2013). This local electrode had a hole with a diameter of 400 μm, and is here designated GLE400, whereas the standard hole has a diameter of 40 μm. Steel B was analyzed with a GLE with the standard 40 μm hole (making it possible to use array samples) and is here designated GLE40. The use of two different hole sizes for the GLE is believed to have minimal influence on the compositional results, although the voltage has to be increased when using a larger hole (Kelly et al., 1996).

The detection rate when using the NLE and the GLEs was 0.002 and 0.001 (ions per pulse), respectively. This means that the actual evaporation rate at the specimen was 3–4 times higher when using the grid with the lower detection efficiency. A higher

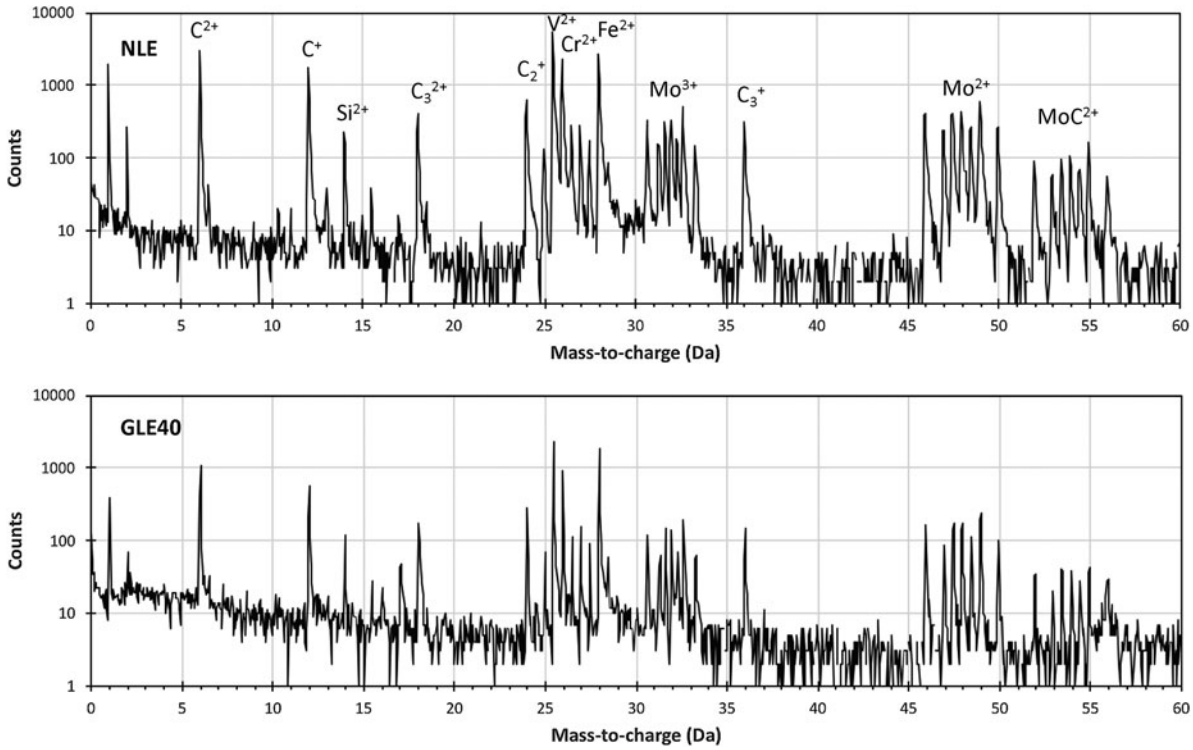

Fig. 3. Mass spectra from carbides in steel B acquired using an NLE (top) and the GLE40 (bottom).

Downloaded from https://www.cambridge.org/core. Chalmers Tekniska Högskola, on 02 Mar 2022 at 11:31:00, subject to the Cambridge Core terms of use, available at https://www.cambridge.org/core/terms. https://doi.org/10.1017/S1431927619000424

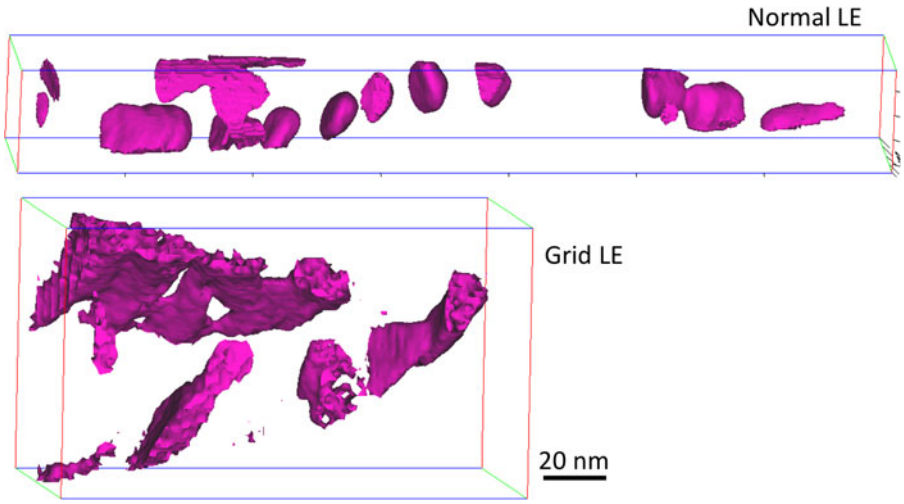

Fig. 4. Reconstructions of steel A, from analyses with an NLE assembly and the GLE400 assembly, showing carbides by isosurfaces using a threshold of C + Mo + V = 30 at.%.

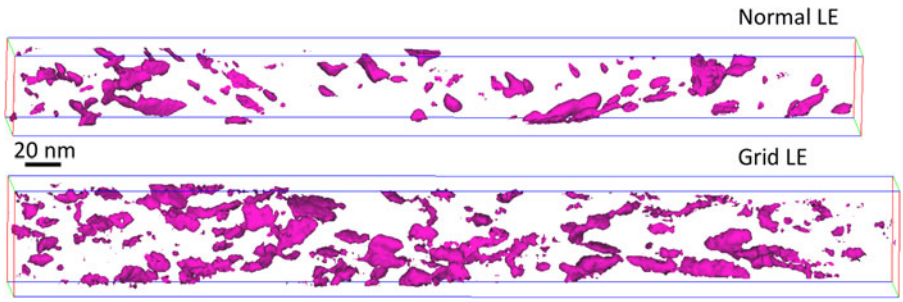

Fig. 5. Reconstructions of steel B, from analyses with an NLE assembly and the GLE40 assembly, showing carbides by isosurfaces using a threshold of C + Mo + V = 30 at.%.

evaporation rate usually gives a small increase in evaporation field, as demonstrated in Figure 1, which shows the voltage (field) increase as a function of evaporation rate for a PSM. Although the rate was increased by a factor of 8 (from 0.005 to 0.04), the voltage only increased by 2.5%, in general agreement with early work by Tsong (1978). This difference in field is not expected to give a significant change in the field evaporation behavior or the occurrence of multiple events (Peng et al., 2017). For Ti–Si–N thin films, Tang et al. (2010) observed a slight increase in the fraction of multiple events when increasing the detection rate by a factor of four, so in the current study the desired decrease in the fraction of multiple events by using a GLE will likely be slightly underestimated.

IVAS 3.6 software (Cameca Inc., Madison, WI, USA) was used for the reconstructions and for evaluating the data. The composition of the carbides was studied using iso-concentration surfaces (isosurfaces). In order to generate the isosurfaces, voxel sizes of $1.0 \times 1.0 \times 1.0$ nm^3 and $1.5 \times 1.5 \times 1.5$ nm^3 were used for analyses obtained with an NLE and the GLE assemblies, respectively. The larger voxel size had to be used to obtain reasonably smooth isosurfaces as the atom density becomes low when the detection efficiency is reduced from 37 to 5%. In both cases the delocalization distances were 3.0 nm in the x–y plane and 2.0 nm in the z direction. In order to evaluate multiple events, epos-files from IVAS were imported into software developed at GPM (University of Rouen, France).

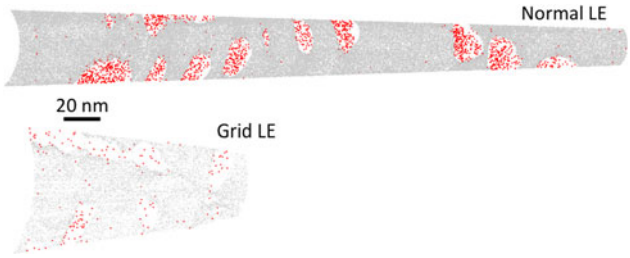

Fig. 6. Atom maps showing all detected Fe (gray) and C (double size, red) atoms in slices of thickness 0.5 nm, of steel A.

Results and Discussion

First, the influence of using a GLE on the detector hit map was studied by analyzing a standard PSM sample. A comparison is shown in Figure 2. It is clear that the grid does not cause any severe image distortions and the (001)-pole is easily recognized in both images.

Steels A and B were analyzed using both an NLE (giving a detection efficiency ~37%) and a GLE (~5%). For steel A, the total fraction of multiple events was 4.2 and 3.0% for the NLE and the GLE400, respectively, whereas for steel B the corresponding numbers were 2.4 and 1.6% for the NLE and the GLE40, respectively. The decrease is relatively small, as the volume

Downloaded from https://www.cambridge.org/core. Chalmers Tekniska Högskola, on 02 Mar 2022 at 11:31:00, subject to the Cambridge Core terms of use, available at https://www.cambridge.org/core/terms. https://doi.org/10.1017/S1431927619000424

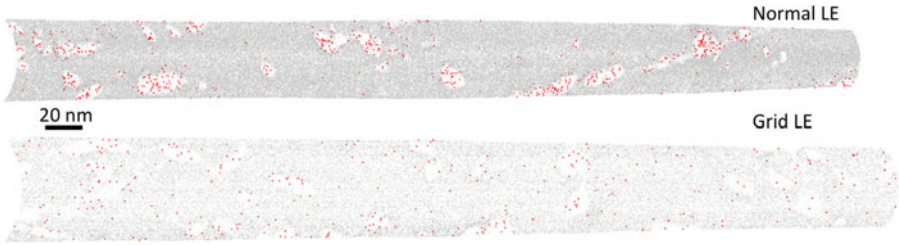

Fig. 7. Atom maps showing all detected Fe (gray) and C (double size, red) atoms in slices of thickness 0.5 nm, of steel B.

fraction of carbides is relatively small, and the atoms from the matrix evaporate mainly as individual ions (singles). However, the relative fraction of multiples decreased with about 30%. The fraction of multiples, if only considering C, was much higher than the values above for all ions. For the NLE, 68 and 66% of the C originated from multiple events for steels A and B, respectively. For the GLE, on the other hand, this fraction was reduced to 29% for both steels.

The mass spectra were typical for analysis of carbide containing steel, with significant peaks from molecular C ions. In Figure 3, mass spectra from the carbides, extracted from the total volume using isosurfaces, are presented. There is not enough signals to deconvolute the presumed overlap between C_2^+ and C_4^{2+} (and there is no sign of any C_2^{2+}). The carbides could possibly contain some nitrogen, but as there is no peak at 7 Da and the peak at 14 Da (which is an overlap with Si^{2+}) is small, the N content is regarded negligible. It can also be seen that the mass spectrum quality was not affected by the type of local electrode used.

Reconstructions of steels A and B, showing isosurfaces generated with a threshold of C + Mo + V = 30 at.%, are presented in Figures 4 and 5, respectively. As expected, the carbides in steel A are larger but fewer, because of coarsening. The sizes and shapes of the carbides vary quite significantly, but there seems to be no difference caused by the use of the grid. However, the interfaces are rougher in the analyses performed with the grid, despite the use of larger voxels. This is clearly a consequence of the lower density of atoms caused by the decreased detection efficiency.

The large difference in atomic density, resulting from the difference in detection efficiency, is illustrated in Figures 6 and 7, which present slices of 0.5 nm thickness, showing all detected Fe and C atoms (each molecular C ion, viz. C_2^+, C_3^+, and C_3^{2+}, is represented by one single dot). The atom density of the carbides is much lower than the density of the matrix, due to strong local magnification effects (Miller & Hetherington, 1991), in turn caused by the higher evaporation field of the carbides (Thuvander et al., 2011; Leitner et al., 2004).

The main focus of the current paper is to investigate the effect of reducing the detection efficiency on the measured C concentration of small secondary carbides. Proximity histograms (proxigrams) of the carbides in steel A (Fig. 4) and in steel B (Fig. 5), are presented in Figures 8 and 9, and it is clear that the measured C concentration is somewhat higher when the grid was used. This is further illustrated in Figure 10, where the C proxigrams are compared. The quantification of the composition of the secondary carbides, determined by using the decomposition tool in IVAS on the ions enclosed by the same isosurfaces as above, is presented in Table 1. The decomposition was primarily used to treat the overlaps of $^{54}Cr/^{54}Fe$ and $^{96}Mo^{2+}/C_4^+$. The measured C concentration of the carbides increased by about 2 at.% for the GLE compared with the NLE, but at the same time the Fe concentration also increased, presumably a consequence of the larger voxel size that had to be used for the GLE data and the rougher isosurfaces. Therefore, it is relevant to compare the compositions measured after removing Fe, and then the increase becomes 4.2 and 6.3 at.% for steels A and B, respectively, see Table 1. Carbide compositions are often corrected by removing elements assumed to belong to the matrix, i.e., mainly Fe (Kolli & Seidman, 2014; Leitner et al., 2004).

It should be noted that the peak at 24 Da has been assigned to C_2^+, although most probably a significant fraction of this peak is C_4^{2+} (Thuvander et al., 2011), as the number of ions (at 24.5 Da) was too low to deconvolute this overlap with any useful precision. As the main focus here is to investigate the effect of detection efficiency on the measured C concentration, it was reasoned that a deconvolution of the 24 Da peak would induce an uncertainty that could obscure the studied effect. However, the fraction of these two ions should be independent of the type of

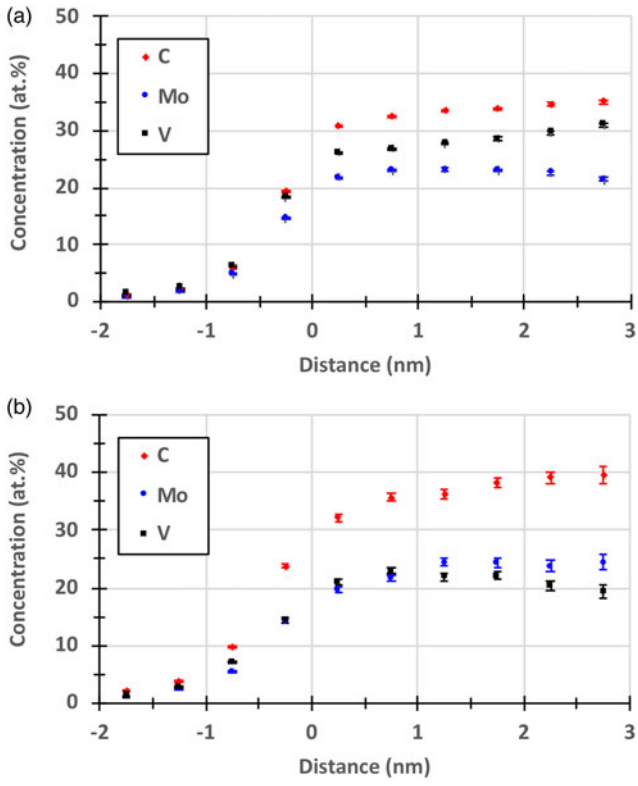

Fig. 8. Proxigrams of carbides in steel A. **a:** Measured with an NLE. **b:** Measured with the GLE400. The error bars (from counting statistics only) for the analysis with the NLE are too small to be visible.

Downloaded from https://www.cambridge.org/core. Chalmers Tekniska Högskola, on 02 Mar 2022 at 11:31:00, subject to the Cambridge Core terms of use, available at https://www.cambridge.org/core/terms. https://doi.org/10.1017/S1431927619000424

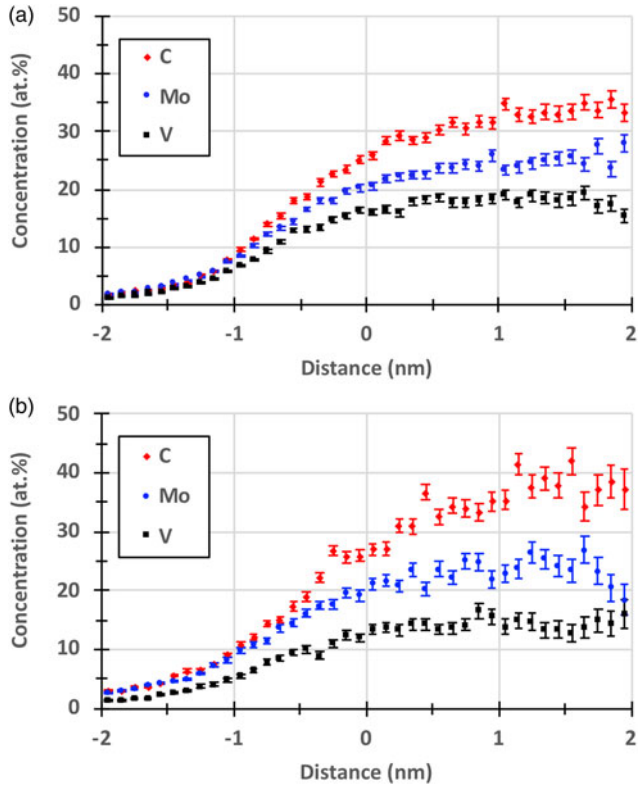

Fig. 9. Proxigrams of carbides in steel B. **a:** Measured with an NLE. **b:** Measured with the GLE40.

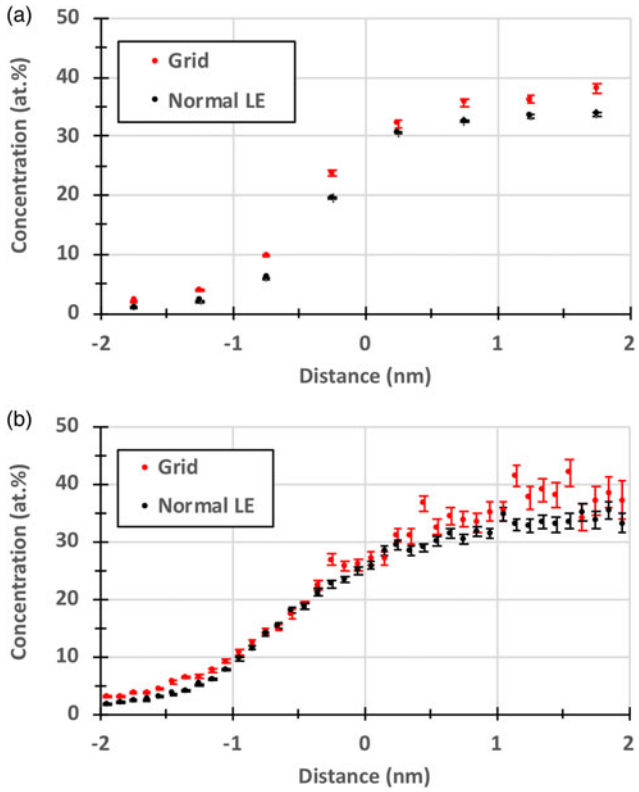

Fig. 10. Proxigrams comparing the measured C concentration obtained with the grid and with an NLE: (**a**) steel A and (**b**) steel B.

Table 1. Composition of Carbides Defined by the Isosurfaces Shown in Figures 4 and 5 (at.%).

	C	Fe	Mo	V	Cr
Steel A, NLE	33.5 ± 0.2	6.1 ± 0.2	21.7 ± 0.2	28.9 ± 0.2	6.4 ± 0.2
Steel A, GLE400	35.5 ± 0.5	11.1 ± 0.6	22.0 ± 0.6	21.2 ± 0.6	6.7 ± 0.6
Steel A, NLE (no Fe)	35.7 ± 0.2	–	23.1 ± 0.2	30.1 ± 0.2	6.8 ± 0.2
Steel A, GLE400 (no Fe)	39.9 ± 0.6	–	24.7 ± 0.7	23.8 ± 0.7	7.5 ± 0.7
Steel B, NLE	31.4 ± 0.8	13.4 ± 1.2	22.7 ± 0.9	18.8 ± 1.0	10.9 ± 1.4
Steel B, GLE40	33.0 ± 1.4	17.8 ± 1.9	16.6 ± 2.0	17.0 ± 1.9	8.6 ± 2.7
Steel B, NLE (no Fe)	37.5 ± 1.0	–	27.1 ± 1.1	22.4 ± 1.2	13.0 ± 1.7
Steel B, GLE40 (no Fe)	43.8 ± 1.8	–	22.1 ± 2.7	22.6 ± 2.5	11.4 ± 3.6

local electrode used. If a deconvolution had been feasible, it would probably have resulted in an increase of the C concentration of a few at.%, resulting in a concentration approaching the expected 45–47 at.% or the ideal stoichiometry of 50 at.%.

The increase in the C concentration when using the GLEs is a clear indication that C is preferentially lost because of multiple events in combination with the detector dead-time (the detector pile-up effect). A further sign of such an effect might be that the C isotope ratios deviate from the natural abundance, as it is unlikely that pairs of an isotope of low abundance are evaporated. The ratio of $^{13}C/^{12}C$ is expected to be 1.08%. For steel A, the measured ratio was 1.27 ± 0.06 and 1.13 ± 0.08% for the C^{2+} and C^{+}, respectively, when using an NLE, whereas the corresponding values for steel B were 1.27 ± 0.08 and 2.29 ± 0.11%. Thus, the isotope ratios indicate that ^{12}C is lost. The reason for the very large $^{13}C^{+}/^{12}C^{+}$ ratio for steel B is unknown, but the presence

Table 2. Fraction of Ions Detected as Multiple Events from the Carbides (%).

	Steel A			Steel B		
	NLE	GLE400	G/N	NLE	GLE40	G/N
C^{2+}	79	43	0.55	70	34	0.49
C^{+}	80	44	0.55	73	34	0.47
C_3^{2+}	76	33	0.43	66	34	0.51
C_2^{+}	84	43	0.51	77	30	0.39
C_3^{+}	91	44	0.49	82	27	0.33
MoC^{2+}	63	21	0.32	45	29	0.64
Mo	75	42	0.56	57	30	0.52
V	56	39	0.69	41	28	0.68

Downloaded from https://www.cambridge.org/core. Chalmers Tekniska Högskola, on 02 Mar 2022 at 11:31:00, subject to the Cambridge Core terms of use, available at https://www.cambridge.org/core/terms. https://doi.org/10.1017/S1431927619000424

Table 3. Multiplicity of Detector Events (%).

	Steel A				Steel B			
	NLE		GLE400		NLE		GLE40	
	Carbide	Matrix	Carbide	Matrix	Carbide	Matrix	Carbide	Matrix
Singles	76.9	98.9	95.6	99.7	79.5	99.4	97.4	99.7
Doubles	16.1	1.1	4.1	0.3	15.8	0.5	2.5	0.23
Triples	4.9	0	0.2	0	3.5	0.06	0.1	0.01
Quadruples	1.4	0	0.03	0	0.8	0.04	0.06	0
Higher	0.7	0	0	0	0.4	0	0	0

of CH^+ could be a contributing cause (Stephan et al., 2015). In the analysis made with GLE40, the corresponding ratios were 1.0 ± 0.2 and $0.9 \pm 0.2\%$ (steel A), and 1.1 ± 0.3 and $1.2 \pm 0.4\%$ (steel B). These values show no deviation from the expected 1.08%, admittedly with a low precision.

In order to extract more information about the evaporation from the carbides, the ions originating from the carbides were studied separately. In Table 2, the fractions of the different ions that were detected in multiple events are listed. The fractions are higher for NLE, and they are roughly halved for GLE. The fractions of ions from multiple events are also larger for steel A, which contains larger carbides. For both steels, when using an NLE, the ions with the highest multiple fraction is C_3^+, followed by C_2^+. The fractions for the large C peaks C^+ and C^{2+} are almost the same, and these fractions are reduced by a similar amount when a GLE was used. The fractions for Mo and V are lower, which agrees with the notion that C is preferentially lost. However, it should be remembered that the losses are not necessarily proportional to the fractions detected in multiple events.

Finally, the multiplicity of the detector events (singles, doubles, triplets, etc.) is presented in Table 3. The data are presented separately for matrix and carbides. As expected, there are more multiple events for the carbides than for the matrix, and there are fewer multiples when using a GLE. In fact, there were no events consisting of more than four ions when using a GLE. It should be noted that the multiplicity values also include un-ranged ions (like hydrogen and background), making, for example, the fraction of single events larger than when looking in Table 2, where only ranged ions are included. Also, for the matrix, the GLE reduced the fraction of multiples, so it could be useful also to study the matrix C concentration with a GLE. However, in the present case the C matrix concentration was too low for obtaining any statistically significant results, in particular as the C content seems to vary between different grains and locations in the microstructure.

The current study has shown that the measured C concentration comes closer to the expected value if the detection efficiency is decreased by inserting a grid in the flight-path of the ions, and that improvements can also be seen for small carbides (~10 nm). As the number of detected ions becomes smaller, the precision decreases (by counting statistics), but more importantly, the accuracy increases, because the number of multiple events (detector pile-up) decreases. In most cases, it of course makes sense to have a high detection efficiency. For example, the possibility of solving mass spectrum overlaps using minor isotopes is reduced with a lower detection efficiency, as noted here for the C_2^+/C_4^{2+} overlap at 24 Da. However, the uncomplicated methodology used here can give important information about any bias caused by multiple events in most material systems and also for small microstructural features, which can be used to develop correction procedures. In many cases it can be useful to perform analyses with an NLE to distinguish small features, determine shapes of small features, perform statistical analyses etc. and with a GLE to obtain complementary information about preferential losses due to detector pile-up effects.

Conclusions

The measurement of the C concentration of secondary MC carbides in two tool steels was found to become more accurate when the detection efficiency was decreased. This was achieved by inserting a grid in the ion flight-path giving a detection efficiency of only 5%. The reason is that the fraction of multiple detector events was decreased and thereby the effect of the detector dead-time was reduced. The methodology presented can give information about preferential losses, due to detector pile-up effects, in APT analysis of any material.

Acknowledgment. Uddeholm AB is acknowledged for providing the material. This research was supported by the Swedish Foundation for Strategic Research (RMA11-0029) and Vinnova (2015-06474). Dr. Hisham Aboulfadl is thanked for performing some of the Si(Sb) analyses.

References

Andersson J (2011). Secondary hardening in some low-chromium hotwork tool steels. PhD Thesis. Chalmers University of Technology, ISBN 978-91-7385-508-2.

Angseryd J, Liu F, Andrén H-O, Gerstl SSA & Thuvander M (2011). Quantitative APT analysis of Ti(C, N). *Ultramicroscopy* **111**, 609–614.

Da Costa G, Wang H, Duguay S, Bostel A, Blavette D & Deconihout B (2012). Advance in multi-hit detection and quantization in atom probe tomography. *Rev Sci Instrum* **83**, 123709.

De Geuser F, Gault B, Bostel A & Vurpillot F (2007). Correlated field evaporation as seen by atom probe tomography. *Surf Sci* **601**, 536–543.

Gault B, Moody MP, Cairney JM & Ringer SP (2012). *Atom Probe Microscopy*. New York, NY, USA: Springer.

Heck PR, Stadermann FJ, Isheim D, Auciello O, Daulton TL, Davis AM, Elam JW, Floss C, Hiller J, Larson DJ, Lewis JB, Mane A, Pellin MJ, Savina MR, Seidman DN & Stephan T (2014). Atom-probe analyses of nanodiamonds from Allende. *Meteoritics and Planetary Science* **49**, 453–467.

Jagutzki O, Cerezo A, Czasch A, Dorner R, Hattas M, Huang M, Mergel V, Spillmann U, Ullmann-Pfleger K, Weber T, Schmidt-Bocking H &

Downloaded from https://www.cambridge.org/core. Chalmers Tekniska Högskola, on 02 Mar 2022 at 11:31:00, subject to the Cambridge Core terms of use, available at https://www.cambridge.org/core/terms. https://doi.org/10.1017/S1431927619000424

Smith GDW (2002). Multiple hit readout of a microchannel plate detector with a three-layer delay-line anode. *IEEE Trans Nucl Sci* **49**, 2477–2483.

Kelly TF, Camus PP, Larson DJ, Holzman LM & Bajikar SS (1996). On the many advantages of local-electrode atom probes. *Ultramicroscopy* **62**, 29–42.

Kinno T, Akutsu H, Tomita M, Kawanaka S, Sonehara T, Hokazono A, Renaud L, Martin I, Benbalagh R, Sallé B & Takeno S (2012). Influence of multi-hit capability on quantitative measurement of NiPtSi thin film with laser-assisted atom probe tomography. *Appl Surf Sci* **259**, 726–730.

Kolli RP & Seidman DN (2014). Co-precipitated and collocated carbides and Cu-rich precipitates in a Fe–Cu steel characterized by atom-probe tomography. *Microsc Microanal* **20**, 1727–1739.

Leitner H, Stiller K, Andren H-O & Danoix F (2004). Conventional and tomographic atom probe investigations of secondary-hardening carbides. *Surf Interface Anal* **36**, 540–545.

Lewis JB, Isheim D, Floss C & Seidman DN (2015). $^{12}C/^{13}C$-ratio determination in nanodiamonds by atom-probe tomography. *Ultramicroscopy* **159**, 248–254.

Marceau RKW, Choi P & Raabe D (2013). Understanding the detection of carbon in austenitic high-Mn steel using atom probe tomography. *Ultramicroscopy* **132**, 239–247.

Martin TL, London AJ, Jenkins B, Hopkin SE, Douglas JO, Styman PD, Bagot PAJ & Moody MP (2017). Comparing the consistency of atom probe tomography measurements of small-scale segregation and clustering between the LEAP 3000 and LEAP 5000 instruments. *Microsc Microanal* **23**, 227–237.

Matoba S, Takahashi R, Io C, Koizumi T & Shiromaru H (2012). Measurement of the absolute sensitivity of a high-sensitivity microchannel plate. *J Phys: Conf Ser* **388**, 142018.

Meisenkothen F, Steel EB, Prosa TJ, Henry KT & Prakash Kolli R (2015). Effects of detector dead-time on quantitative analyses involving boron and multi-hit detection events in atom probe tomography. *Ultramicroscopy* **159**, 101–111.

Miller MK & Forbes RG (2014). *Atom-Probe Tomography: The Local Electrode Atom Probe*. New York, NY, USA: Springer.

Miller MK & Hetherington MG (1991). Local magnification effects in the atom probe. *Surf Sci* **241**, 442–449.

Müller M, Gault B, Smith GDW & Grovenor CRM (2011). Accuracy of pulsed laser atom probe tomography for compound semiconductor analysis. *J Phys: Conf Ser* **326**, 012031.

Peng Z, Choi P, Li Y, Gault B & Raabe D (2017). Evaluation of analysis conditions for laser-pulsed atom probe tomography: Examples of cemented tungsten carbide. *Microsc Microanal* **23**, 431–442.

Peng Z, Vurpillot F, Choi P, Li Y, Raabe D & Gault B (2018). On the detection of multiple events in atom probe tomography. *Ultramicroscopy* **189**, 54–60.

Prosa TJ, Geiser BP, Lawrence DJ, Olsen JD & Larson DJ (2014). Developing detection efficiency standards for atom probe tomography. In *Proceedings of* SPIE 9173, Instrumentation, Metrology, and Standards for Nanomanufacturing, Optics and Semiconductors VIII, 917307. San Diego, CA, USA.

Rolander U & Andrén H-O (1989). Statistical correction for pile-up in the atom-probe detector system. *Le Journal de Physique Colloques* **50**, C8–529–C8-534.

Saxey DN (2011). Correlated ion analysis and the interpretation of atom probe mass spectra. *Ultramicroscopy* **111**, 473–479.

Stephan T, Heck PR, Isheim D & Lewis JB (2015). Correction of dead time effects in laser-induced desorption time-of-flight mass spectrometry: Applications in atom probe tomography. *Int J Mass Spectrom* **379**, 46–51.

Tang F, Gault B, Ringer SP & Cairney JM (2010). Optimization of pulsed laser atom probe (PLAP) for the analysis of nanocomposite Ti–Si–N films. *Ultramicroscopy* **110**, 836–843.

Thuvander M, Kvist A, Johnson LJS, Weidow J & Andrén H-O (2013). Reduction of multiple hits in atom probe tomography. *Ultramicroscopy* **132**, 81–85.

Thuvander M, Weidow J, Angseryd J, Falk LKL, Liu F, Sonestedt M, Stiller K & Andrén H-O (2011). Quantitative atom probe analysis of carbides. *Ultramicroscopy* **111**, 604–608.

Toth LE (1971). Transition Metal Carbides and Nitrides. New York: Academic Press (Refractory materials, vol. 7).

Tsong TT (1978). Measurement of the field evaporation rate of several transition metals. *J Phys F* **8**, 1349–1352.

Yao L, Gault B, Cairney JM & Ringer SP (2012). On the multiplicity of field evaporation events in atom probe: A new dimension to the analysis of mass spectra. *Philos Mag Lett* **90**, 121–129.

Downloaded from https://www.cambridge.org/core. Chalmers Tekniska Högskola, on 02 Mar 2022 at 11:31:00, subject to the Cambridge Core terms of use, available at https://www.cambridge.org/core/terms. https://doi.org/10.1017/S1431927619000424